Available online at www.sciencedirect.com
SCIENCE DIRECT®
Journal of Computational Physics 203 (2005) 1–21
JOURNAL OF COMPUTATIONAL PHYSICS
www.elsevier.com/locate/jcp

A non-overlapping domain decomposition method with non-matching grids for modeling large finite antenna arrays ☆

Seung-Cheol Lee *, Marinos N. Vouvakis, Jin-Fa Lee

ElectroScience Laboratory, Electrical Engineering Department, The Ohio State University, 1320 Kinnear Road, Columbus 43212, USA

Received 3 June 2004; received in revised form 9 August 2004; accepted 9 August 2004
Available online 17 September 2004

Abstract

A non-overlapping domain decomposition method (DDM) is proposed herein to solve Maxwell equations in $\mathbb{R}^3$. In this work, the Maxwell equations are discretized using a vector finite element method with hierarchical **H**(curl) vector basis functions. There are two major ingredients in the proposed non-overlapping DDM: (a) A proper 1st order transmission condition to enforce field continuity across domain boundaries and (b) A cement technique to allow non-matching grids for neighboring domains. Moreover, a detail Fourier analysis of the transmission condition for a canonical half-space example is presented. The analysis provides significant insights into the convergence behavior of the proposed non-overlapping DDM for solving electromagnetic radiation problems, such as the large finite antenna arrays. Particularly for the antenna arrays, the proposed non-overlapping DDM is extremely efficient since the formulation can easily incorporate geometrical repetitions. Exponentially tapered notch (Vivaldi) antenna arrays with size up to 100×100 elements are solved on a common PC to validate the proposed non-overlapping DDM.

Keywords: Domain decomposition methods; Transmission conditions; Maxwell's equations

1. Introduction

Modern wireless communication systems and radars often use large antenna arrays to transmit and/or receive signals through space. These arrays are usually geometrically complex, include significant number of antenna elements, and are electrically large. Consequently, it is of great challenge to model such structures

☆ This work is jointly sponsored by Ansoft Corp. through two Ansoft fellowships and Temasek Lab., National University of Singapore, Singapore.
* Corresponding author. Tel.: +1 614 292 7981.
E-mail addresses: lee.1802@osu.edu (S.-C. Lee), vouvakis.1@osu.edu (M.N. Vouvakis), jinlee@ee.eng.ohio-state.edu (J.-F. Lee).

0021-9991/$ - see front matter
doi:10.1016/j.jcp.2004.08.004

using numerical methods. Without parallelization, it would be prohibitive to solve large finite antenna arrays using traditional methods, such as finite element (FE) [1], integral equation (IE) [2] and finite difference time domain (FDTD) [3] methods. However, due to many repetitions in the structure, it is natural to apply DDMs to model large finite antenna arrays.

Every DDM algorithm starts by dividing the computational domain into a number of smaller sub-domains [4]. The sub-domains are solved individually and the interactions between the sub-domains are communicated through a proper transmission condition (TC) [5–7]. This process is applied iteratively until the entire solution converges to a desired accuracy. Based on this simple framework, various methods have been proposed for different types of problems or differential equations. The classical alternating Schwarz method [4,8,9] is based on overlapping sub-domains with Dirichlet type TCs. The method is used primarily for elliptic equations. Although the overlapping DDM is still an active research topic with many preferable features, the non-overlapping DDM has become very appealing for its inherent parallelism and flexibility [10]. Recent works have found that the convergence of the non-overlapping DDM can be assured by imposing Robin type TC; we refer [5,11] for elliptic problems, whereas for hyperbolic problems we state [6,7,12]. Furthermore, Maxwell's problems have been successfully solved using the non-overlapping DDM that employs Robin TCs [13–16]. The first non-overlapping DDM for Maxwell equations was proposed by Després in [13,14], and extended to a relaxed iteration scheme and a higher order TC by Collino et al. [15]. In these works, pseudo-energy norms were used to prove the convergence of their methods. However, we shall prove convergence of our non-overlapping DDM through a Fourier analysis, which is more related to physics. Our analysis follows closely the work of Gander et al. [6], where the convergence rate is derived for simplified semi-infinite domains. With the Fourier analysis for semi-infinite domains, analytical expressions of the convergence factors can be obtained. Therefore, one of the main focuses of this paper is a comprehensive study of the effects of TCs in solving general 3D electromagnetic (EM) problems using the non-overlapping DDM.

The present method also allows *non-matching* grids between neighboring sub-domains to enable independent local discretizations. The flexibility of non-matching discretizations across sub-domains not only relaxes the mesh generation and adaptive mesh refinement process, but more importantly avoids the periodic mesh constraints on the sides of the repeating blocks. A popular approach to address the non-matching grids issue in the non-overlapping DDMs is the mortar element method. The mortar element method described in [9,22,23] accounts for the non-conformity between domains via the Lagrangian multiplier. The main drawbacks of the mortar elements are two: (a) the Lagrangian multipliers thus introduced do not relate to any physical quantities and (b) zero diagonal blocks are resulted in the final matrix equations. In our approach, the non-matching grids are permissible through the introduction of an additional set of variables on each sub-domain interface. Unlike the mortar element method, the additional variables introduced in the current approach possess physical meaning, and do not result in zero diagonal blocks in the final matrix equation. Subsequently, our method is closely related to the cement method described in [18]. Similar approaches are also found in [17,19–21].

To solve the sub-domain problems, the finite element method (FEM) is employed. The capability of FEM to handle complex geometries and highly inhomogeneous material properties is of paramount importance to simulate any real-life antenna array problems. In the current approach, we adopt the second-order hierarchical Nedelec $\mathbf{H}(\mathrm{curl})$ tetrahedral vector finite elements [24]. Also, we apply the p-type multiplicative Schwarz (pMUS) preconditioner presented in [4,25] to solve the sub-domain matrix equations. Moreover, in order to assure the robustness and the accuracy of the entire solution process, the discrete Hodge decomposition [26] and the *h*-adaptive mesh refinement (*h*-AMR) scheme [27] are also incorporated.

The rest of the paper is organized as follows. We first describe the continuous boundary value problem (BVP) in Section 2.1. The decomposed BVP used in the DDM is presented in Section 2.2. In Section 2.3, the cement method for electromagnetic problems is discussed in detail. Section 2.4 presents the convergence rate analyses of the Robin TCs for three dimensional semi-infinite domains with planar interfaces. The pro-

posed DDM is reformulated in Section 2.5 to provide additional insights of the algorithm. The numerical results, large finite Vivaldi antenna arrays, are included in Section 3 to demonstrate the versatility and elegancy of the proposed non-overlapping DDM. Finally, a brief summary and conclusion is included in Section 4.

2. Theory

2.1. Problem statement

In this paper, we are interested in solving large finite antenna arrays. A sample example is shown in Fig. 1, where an $n \times m$ Vivaldi antenna array is plotted. Moreover, as indicated in Fig. 1, we enclosed the entire array in a bounded domain Ω. Subsequently, the mathematical model can be described by:

$$\begin{aligned}
&\nabla \times \frac{1}{\mu_r} \nabla \times \mathbf{E} - k^2 \varepsilon_r \mathbf{E} = -\mathrm{j}\omega\mu_0 \mathbf{J}^{\mathrm{imp}} \quad \text{in } \mathbb{R}^3, \\
&\mathbf{n} \times \nabla \times \mathbf{E} = 0 \quad \text{on } \Gamma_{\mathrm{pmc}}, \\
&\mathbf{n} \times \mathbf{E} = 0 \quad \text{on } \Gamma_{\mathrm{pec}}, \\
&\lim_{r \to \infty} (r \nabla \times \mathbf{E} + \mathrm{j}k\mathbf{r} \times \mathbf{E}) = 0, \quad r = |\mathbf{r}| = \sqrt{x^2 + y^2 + z^2},
\end{aligned} \tag{1}$$

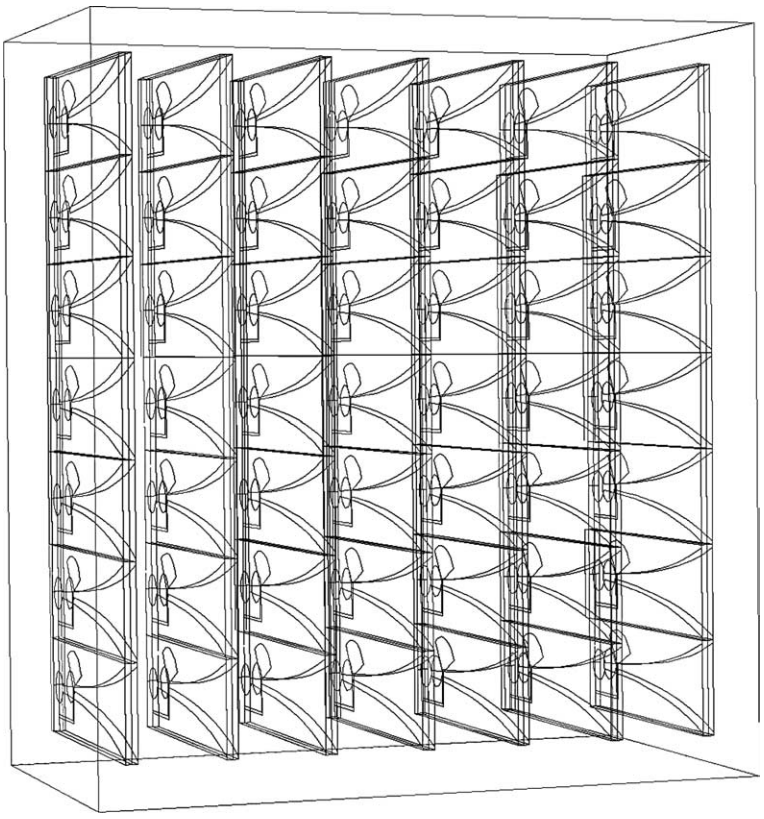

Fig. 1. Geometry of a finite $n \times m$ Vivaldi antenna array.

where k refers to the wave number, the unit normal $\mathbf{n}$ is always pointing away from the problem domain, and ε_r and μ_r are the relative permittivity and permeability of the medium, respectively. Note also that throughout this paper, vector entities are written in bold letters. The perfect magnetic conductors (PMC) and the perfect electric conductors (PEC) are denoted by Γ_{pmc} and Γ_{pec}, respectively. The excitation is assumed to be an impressed electric current $\mathbf{J}^{\text{imp}}$ within the domain of interest. The last equation in (1) is the Silver–Muller radiation condition. However, in our current approach, we simply employ the 1st order absorbing boundary condition (ABC) [28] on Γ_∞ to convert the infinite domain problem to a finite one. Subsequently, the boundary value problem (BVP) can be stated as

$$\begin{aligned}
&\nabla \times \frac{1}{\mu_r}\nabla \times \mathbf{E} - k^2\varepsilon_r\mathbf{E} = -\mathrm{j}\omega\mu_0\mathbf{J}^{\text{imp}} \quad \text{in } \Omega \subset \mathbb{R}^3,\\
&\gamma_{\text{t}}^{\times}(\nabla \times \mathbf{E}) = 0 \quad \text{on } \Gamma_{\text{pmc}},\\
&\gamma_{\text{t}}(\mathbf{E}) = 0 \quad \text{on } \Gamma_{\text{pec}},\\
&\gamma_{\text{t}}^{\times}(\nabla \times \mathbf{E}) - \mathrm{j}k\gamma_{\text{t}}(\mathbf{E}) = 0 \quad \text{on } \Gamma_\infty,
\end{aligned} \tag{2}$$

where the tangential surface trace γ_{t} and the twisted tangential surface trace $\gamma_{\text{t}}^{\times}$ operators are defined by

$$\begin{aligned}
&\gamma_{\text{t}}(\mathbf{u}) = \mathbf{n} \times \mathbf{u} \times \mathbf{n},\\
&\gamma_{\text{t}}^{\times}(\mathbf{u}) = \mathbf{n} \times \mathbf{u}.
\end{aligned} \tag{3}$$

The corresponding Galerkin weak formulation for (2) can now be formally stated as

$$\begin{aligned}
&\text{Seek } \mathbf{u}^h \in S^h \subset \mathbf{H}_0\big(\text{curl}; \Omega^h\big) \text{ such that}\\
&\int_{\Omega^h} \nabla \times \mathbf{v}^h \cdot \frac{1}{\mu_r}\nabla \times \mathbf{u}^h \,\mathrm{d}V - k^2 \int_{\Omega^h} \mathbf{v}^h \cdot \varepsilon_r\mathbf{u}^h \,\mathrm{d}V + \frac{\mathrm{j}k}{\eta}\int_{\Gamma_\infty} \mathbf{v}^h \cdot \gamma_{\text{t}}\big(\mathbf{u}^h\big)\,\mathrm{d}S = -\mathrm{j}\omega\mu_0 \int_{\Omega^h} \mathbf{v}^h \cdot \mathbf{J}^{\text{imp}}\,\mathrm{d}V\\
&\forall \mathbf{v}^h \in S^h \subset \mathbf{H}_0\big(\text{curl}; \Omega^h\big)
\end{aligned}$$

where Ω^h is a discretization of the finite domain Ω by tetrahedra with typical element size h and $\mathbf{H}_0(\text{curl}; \Omega^h)$ is the usual curl-conforming function space, namely

$$\mathbf{H}_0\big(\text{curl}; \Omega^h\big) = \Big\{\mathbf{v}\,|\,\mathbf{v} \in \big(L^2\big(\Omega^h\big)\big)^3, (\nabla \times \mathbf{v}) \in \big(L^2\big(\Omega^h\big)\big)^3 \text{ and } \gamma_{\text{t}}(\mathbf{v}) = 0 \text{ on } \Gamma_{\text{pec}}\Big\}. \tag{4}$$

2.2. A non-overlapping domain decomposition algorithm

The solution of large finite antenna arrays naturally suggests the application of the DDM. For simplicity and without loss of generality, we consider only partitioning the problem domain into two sub domains. As shown in Fig. 2, the particular DDM that we are interested in this application is the non-overlapping DDM. Thus the problem domain Ω is partitioned into two non-overlapping sub-domains, Ω_1 and Ω_2.

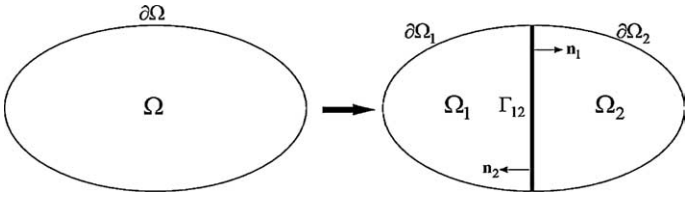

Fig. 2. Partitioning a domain Ω into two non-overlapping sub-domains Ω_1 and Ω_2.

We shall denote the boundary that separates Ω_1 and Ω_2 by Γ_{12}. Moreover, we shall also employ $\mathbf{E}_1$ and $\mathbf{E}_2$ to denote the restrictions of $\mathbf{E}$ in sub-domains Ω_1 and Ω_2, respectively. Subsequently, the proposed non-overlapping DDM can be formulated through the following iteration process:

find $(\mathbf{E}_1^{(n)}, \mathbf{E}_2^{(n)})$ given an arbitrary initial guess $(\mathbf{E}_1^{(0)}, \mathbf{E}_2^{(0)})$ by BVP for $(\mathbf{E}_1^{(n)})$ in sub − domain Ω_1

$$\begin{aligned}
&\nabla \times \frac{1}{\mu_r} \nabla \times \mathbf{E}_1^{(n)} - k^2 \varepsilon_r \mathbf{E}_1^{(n)} = -\mathrm{j}\omega\mu_0 \mathbf{J}_1^{\mathrm{imp}} \quad \text{in } \Omega_1,\\
&\gamma_{\mathrm{t}}\left(\mathbf{E}_1^{(n)}\right) = 0 \quad \text{on } \partial\Omega_1 \cap \Gamma_{\mathrm{pec}},\\
&\gamma_{\mathrm{t}}^{\times}\left(\frac{1}{\mu_r} \nabla \times \mathbf{E}_1^{(n)}\right) = 0 \quad \text{on } \partial\Omega_1 \cap \Gamma_{\mathrm{pmc}},\\
&\gamma_{\mathrm{t}}^{\times}\left(\frac{1}{\mu_r} \nabla \times \mathbf{E}_1^{(n)}\right) - \mathrm{j}k\gamma_{\mathrm{t}}\left(\mathbf{E}_1^{(n)}\right) = 0 \quad \text{on } \partial\Omega_1 \cap \Gamma_{\infty},\\
&\gamma_{\mathrm{t}}^{\times}\left(\frac{1}{\mu_r} \nabla \times \mathbf{E}_1^{(n)}\right)_{\Gamma_{12}^{(1)}} - \mathrm{j}k\gamma_{\mathrm{t}}\left(\mathbf{E}_1^{(n)}\right) = -\gamma_{\mathrm{t}}^{\times}\left(\frac{1}{\mu_r} \nabla \times \mathbf{E}_2^{(n-1)}\right)_{\Gamma_{12}^{(2)}} - \mathrm{j}k\gamma_{\mathrm{t}}\left(\mathbf{E}_2^{(n-1)}\right) \quad \text{on } \Gamma_{12}
\end{aligned} \tag{5}$$

and the BVP for $\mathbf{E}_2^{(n)}$ in sub-domain Ω_2

$$\begin{aligned}
&\nabla \times \frac{1}{\mu_r} \nabla \times \mathbf{E}_2^{(n)} - k^2 \varepsilon_r \mathbf{E}_2^{(n)} = -\mathrm{j}\omega\mu_0 \mathbf{J}_2^{\mathrm{imp}} \quad \text{on } \Omega_2,\\
&\gamma_{\mathrm{t}}\left(\mathbf{E}_2^{(n)}\right) = 0 \quad \text{on } \partial\Omega_2 \cap \Gamma_{\mathrm{pec}},\\
&\gamma_{\mathrm{t}}^{\times}\left(\frac{1}{\mu_r} \nabla \times \mathbf{E}_2^{(n)}\right) = 0 \quad \text{on } \partial\Omega_2 \cap \Gamma_{\mathrm{pmc}},\\
&\gamma_{\mathrm{t}}^{\times}\left(\frac{1}{\mu_r} \nabla \times \mathbf{E}_2^{(n)}\right) - \mathrm{j}k\gamma_{\mathrm{t}}\left(\mathbf{E}_2^{(n)}\right) = 0 \quad \text{on } \partial\Omega_2 \cap \Gamma_{\infty},\\
&\gamma_{\mathrm{t}}^{\times}\left(\frac{1}{\mu_r} \nabla \times \mathbf{E}_2^{(n)}\right)_{\Gamma_{12}^{(2)}} - \mathrm{j}k\gamma_{\mathrm{t}}\left(\mathbf{E}_2^{(n)}\right) = -\gamma_{\mathrm{t}}^{\times}\left(\frac{1}{\mu_r} \nabla \times \mathbf{E}_1^{(n-1)}\right)_{\Gamma_{12}^{(1)}} - \mathrm{j}k\gamma_{\mathrm{t}}\left(\mathbf{E}_1^{(n-1)}\right) \quad \text{on } \Gamma_{12}.
\end{aligned} \tag{6}$$

In Eqs. (5) and (6), we define $\gamma_{\mathrm{t}}^{\times}(\mathbf{u})_{\Gamma^{(i)}} = \mathbf{n}_i \times \mathbf{u}$, where $\mathbf{n}_i$ is the unit normal on the interface boundary Γ_{12} and pointing away from sub-domain Ω_i (refer to Fig. 2). Also, we remark that in our current implementation, we have employed the Robin condition as the TC between the two sub-domains. It is straightforward to show that the two transmission conditions in (5) and (6) imply the needed field continuities across Γ_{12}. Namely,

$$\begin{aligned}
&\begin{cases}
\gamma_{\mathrm{t}}^{\times}\left(\frac{1}{\mu_r} \nabla \times \mathbf{E}_1^{(n)}\right)_{\Gamma_{12}^{(1)}} - \mathrm{j}k\gamma_{\mathrm{t}}\left(\mathbf{E}_1^{(n)}\right) = -\gamma_{\mathrm{t}}^{\times}\left(\frac{1}{\mu_r} \nabla \times \mathbf{E}_2^{(n-1)}\right)_{\Gamma_{12}^{(2)}} - \mathrm{j}k\gamma_{\mathrm{t}}\left(\mathbf{E}_2^{(n-1)}\right) & \text{on } \Gamma_{12},\\
\gamma_{\mathrm{t}}^{\times}\left(\frac{1}{\mu_r} \nabla \times \mathbf{E}_2^{(n)}\right)_{\Gamma_{12}^{(2)}} - \mathrm{j}k\gamma_{\mathrm{t}}\left(\mathbf{E}_2^{(n)}\right) = -\gamma_{\mathrm{t}}^{\times}\left(\frac{1}{\mu_r} \nabla \times \mathbf{E}_1^{(n-1)}\right)_{\Gamma_{12}^{(1)}} - \mathrm{j}k\gamma_{\mathrm{t}}\left(\mathbf{E}_1^{(n-1)}\right) & \text{on } \Gamma_{12},
\end{cases}\\
&\qquad \Rightarrow \begin{cases}
\gamma_{\mathrm{t}}^{\times}\left(\frac{1}{\mu_r} \nabla \times \mathbf{E}_1\right)_{\Gamma_{12}^{(1)}} = -\gamma_{\mathrm{t}}^{\times}\left(\frac{1}{\mu_r} \nabla \times \mathbf{E}_2\right)_{\Gamma_{12}^{(2)}}\\
\gamma_{\mathrm{t}}(\mathbf{E}_1) = \gamma_{\mathrm{t}}(\mathbf{E}_2)
\end{cases}
\end{aligned} \tag{7}$$

We shall show later, by Fourier analysis, that the use of the Robin condition will provide the needed convergence for the propagating modes.

2.3. DDM with non-matching grids

The DDM suggested by Eqs. (5) and (6) requires a matching grid between the sub-domains Ω_1 and Ω_2. Practically, this requirement taxes significantly on the numerical analyst when he/she tries to analyze large finite antenna arrays. In this paper, we propose a novel approach, similar to the cement techniques employed in the literature [17,18], for DDM with non-matching grids. With the proposed technique, each sub-domain can be meshed independently without consideration of conformity to the adjacent sub-domains (see Fig. 3). Note also in Fig. 3, the interface boundary Γ_{ij} between the sub-domains Ω_i and Ω_j has been split into two identical boundary surfaces, Γ_i (resides on Ω_i) and Γ_j (resides on Ω_j). It is due to this splitting that different triangulations are allowed to exist on Γ_i and Γ_j. The boundary conditions, tangential continuities of both electric and magnetic fields across Γ_{ij}, will be imposed through a Galerkin variational treatment. Although in principle, the triangulations in Γ_i and Γ_j can be drastically different, the rule of thumb is that the spatial resolutions h_i (the characteristic element size in triangulation T_{h_i}) and h_j (the characteristic element size in triangulation T_{h_j}) should be compatible to assure the accuracy.

To implement the cement method, which *glues* together the non-matching grids in the DDMs, we introduce additional sets of variables on the interface boundaries. For simplicity, we consider again the two sub-domain DDMs as shown in Fig. 4. As can be seen in Fig. 4, we have employed two separate sets of tangential traces, $\mathbf{e}_1$ and $\mathbf{e}_2$, of the electric fields on Γ_1 and Γ_2, respectively. Additionally, there are two new sets of variables, $\mathbf{J}_1$ and $\mathbf{J}_2$, defined on the interface boundary. Subsequently, at the nth iteration, our two BVPs (5) and (6) can now be restated as:

$$
\begin{aligned}
&\nabla \times \frac{1}{\mu_r} \nabla \times \mathbf{E}_1^{(n)} - k^2 \varepsilon_r \mathbf{E}_1^{(n)} = -\mathrm{j}\omega\mu_0 \mathbf{J}_1^{\mathrm{imp}} \quad \text{in } \Omega_1,\\
&\gamma_{\mathrm{t}}\left(\mathbf{E}_1^{(n)}\right) = 0 \quad \text{on } \partial\Omega_1 \cap \Gamma_{\mathrm{pec}},\\
&\gamma_{\mathrm{t}}^{\times}\left(\frac{1}{\mu_r} \nabla \times \mathbf{E}_1^{(n)}\right) = 0 \quad \text{on } \partial\Omega_1 \cap \Gamma_{\mathrm{pmc}},\\
&\gamma_{\mathrm{t}}^{\times}\left(\frac{1}{\mu_r} \nabla \times \mathbf{E}_1^{(n)}\right) - \mathrm{j}k\gamma_{\mathrm{t}}\left(\mathbf{E}_1^{(n)}\right) = 0 \quad \text{on } \partial\Omega_1 \cap \Gamma_{\infty},\\
&\mathbf{J}_1^{(n)} = \gamma_{\mathrm{t}}^{\times}\left(\frac{1}{\mu_r} \nabla \times \mathbf{E}_1^{(n)}\right)_{\Gamma_1} \quad \text{on } \Gamma_1,\\
&\mathbf{J}_1^{(n)} - \mathrm{j}k\mathbf{e}_1^{(n)} = -\mathbf{J}_2^{(n-1)} - \mathrm{j}k\mathbf{e}_2^{(n-1)} \quad \text{on } \Gamma_1
\end{aligned}
\tag{8}
$$

and

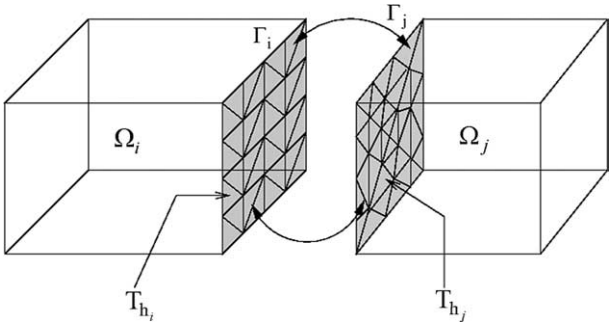

Fig. 3. Cement technique glues together two sub-domains Ω_i and Ω_j with non-matching surface grids.

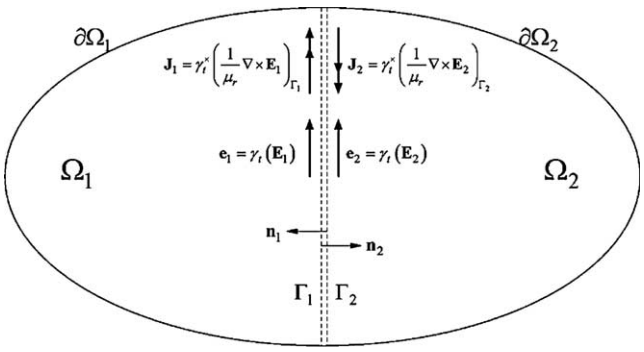

Fig. 4. Auxiliary variables for non-matching grid domain decomposition methods.

$$
\begin{aligned}
&\nabla\times\frac{1}{\mu_r}\nabla\times\mathbf{E}_2^{(n)} - k^2\varepsilon_r\mathbf{E}_2^{(n)} = -\mathrm{j}\omega\mu_0\mathbf{J}_2^{\mathrm{imp}} \quad \text{in } \Omega_2,\\
&\gamma_t\left(\mathbf{E}_2^{(n)}\right) = 0 \quad \text{on } \partial\Omega_2\cap\Gamma_{\mathrm{pec}},\\
&\gamma_t^{\times}\left(\frac{1}{\mu_r}\nabla\times\mathbf{E}_2^{(n)}\right) = 0 \quad \text{on } \partial\Omega_2\cap\Gamma_{\mathrm{pmc}},\\
&\gamma_t^{\times}\left(\frac{1}{\mu_r}\nabla\times\mathbf{E}_2^{(n)}\right) - \mathrm{j}k\gamma_t\left(\mathbf{E}_2^{(n)}\right) = 0 \quad \text{on } \partial\Omega_2\cap\Gamma_{\infty},\\
&\mathbf{J}_2^{(n)} = \gamma_t^{\times}\left(\frac{1}{\mu_r}\nabla\times\mathbf{E}_2^{(n)}\right)_{\Gamma_2} \quad \text{on } \Gamma_2,\\
&\mathbf{J}_2^{(n)} - \mathrm{j}k\mathbf{e}_2^{(n)} = -\mathbf{J}_1^{(n-1)} - \mathrm{j}k\mathbf{e}_1^{(n-1)} \quad \text{on } \Gamma_2.
\end{aligned}
\tag{9}
$$

It is obvious that when Eqs. (8) and (9) converge, the converged fields $\mathbf{E}_1$ and $\mathbf{E}_2$ are indeed the restrictions of the electric field $\mathbf{E}$ of (2) in the sub-domains Ω_1 and Ω_2, respectively. We should emphasize here that the two sets of variables $\mathbf{J}_1$ and $\mathbf{J}_2$ defined on Γ_1 and Γ_2 are the key ingredients of the cement technique that we introduce here. Unlike the Lagrange multipliers in the mortar element method, the additional variables carry significant physical meanings; namely, they are proportional to the electric current density on the surfaces. Furthermore, they will not result in any zero diagonal blocks in the final matrix equations.

To implement the domain decomposition iteration described by Eqs. (8) and (9), we need to employ finite dimensional descriptions for Ω_1 and Ω_2. In the current implementation, we have chosen to discretize Ω_1 and Ω_2 into unions of tetrahedra. The corresponding spaces for the fields and the additional variables are

$$
\begin{aligned}
&\mathbf{E}_1 \in \mathbf{S}_1^h \subset \mathbf{H}_0(\mathrm{curl};\Omega_1), \quad \mathbf{E}_2 \in \mathbf{S}_2^h \subset \mathbf{H}_0(\mathrm{curl};\Omega_2),\\
&\mathbf{J}_1 \in \mathbf{\Lambda}_1^h \subset \mathbf{H}_{\|}^{-1/2}(\mathrm{div}_{\Gamma};\Gamma_1), \quad \mathbf{J}_2 \in \mathbf{\Lambda}_2^h \subset \mathbf{H}_{\|}^{-1/2}(\mathrm{div}_{\Gamma};\Gamma_2).
\end{aligned}
\tag{10}
$$

Specifically, the basis functions for $\mathbf{E}_1$, $\mathbf{E}_2$ within each tetrahedron are the $p = 2$, 1st kind Nedelec $\mathbf{H}(\mathrm{curl})$ vector elements [24]. Moreover, for the variables, $\mathbf{J}_1$ and $\mathbf{J}_2$, the basis functions are the $p = 2$, 1st kind Nedelec $\mathbf{H}(\mathrm{div})$ vector elements [29] on triangles. Consequently, the corresponding Galerkin weak statement for Eqs. (8) and (9) is:

$$
\begin{aligned}
&\text{Seek } (\mathbf{E}_1^{(n)}, \mathbf{E}_2^{(n)}) \in \mathbf{S}_1^h \times \mathbf{S}_2^h \text{ and } (\mathbf{J}_1^{(n)}, \mathbf{J}_2^{(n)}) \in \mathbf{\Lambda}_1^h \times \mathbf{\Lambda}_2^h \text{ such that} \\
&a\left(\mathbf{v}_1^h, \mathbf{E}_1^{(n)}\right)_{\Omega_1} + \mathrm{j}k\left(\gamma_t \mathbf{v}_1^h, \mathbf{e}_1^{(n)}\right)_{\partial\Omega_1 \cap \Gamma_\infty} + \left(\gamma_t \mathbf{v}_1^h, \mathbf{J}_1^{(n)}\right)_{\Gamma_1} = \frac{-\mathrm{j}k}{\eta}\left(\mathbf{v}_1^h, \mathbf{J}_1^{\mathrm{imp}}\right)_{\Omega_1}, \\
&a\left(\mathbf{v}_2^h, \mathbf{E}_2^{(n)}\right)_{\Omega_2} + \mathrm{j}k\left(\gamma_t \mathbf{v}_2^h, \mathbf{e}_2^{(n)}\right)_{\partial\Omega_2 \cap \Gamma_\infty} + \left(\gamma_t \mathbf{v}_2^h, \mathbf{J}_2^{(n)}\right)_{\Gamma_2} = \frac{-\mathrm{j}k}{\eta}\left(\mathbf{v}_2^h, \mathbf{J}_2^{\mathrm{imp}}\right)_{\Omega_2}, \\
&\left(\boldsymbol{\lambda}_1^h, \mathbf{e}_1^{(n)}\right)_{\Gamma_1} + \frac{\mathrm{j}}{k}\left(\boldsymbol{\lambda}_1^h, \mathbf{J}_1^{(n)}\right)_{\Gamma_1} = \left(\boldsymbol{\lambda}_1^h, \mathbf{e}_2^{(n-1)}\right)_{\Gamma_1} - \frac{\mathrm{j}}{k}\left(\boldsymbol{\lambda}_1^h, \mathbf{J}_2^{(n-1)}\right)_{\Gamma_1}, \\
&\left(\boldsymbol{\lambda}_2^h, \mathbf{e}_2^{(n)}\right)_{\Gamma_2} + \frac{\mathrm{j}}{k}\left(\boldsymbol{\lambda}_2^h, \mathbf{J}_2^{(n)}\right)_{\Gamma_2} = \left(\boldsymbol{\lambda}_2^h, \mathbf{e}_1^{(n-1)}\right)_{\Gamma_2} - \frac{\mathrm{j}}{k}\left(\boldsymbol{\lambda}_2^h, \mathbf{J}_1^{(n-1)}\right)_{\Gamma_2}, \\
&\quad \forall\left(\mathbf{v}_1^h, \mathbf{v}_2^h\right) \in \mathbf{S}_1^h \times \mathbf{S}_2^h \quad \text{and} \quad \left(\boldsymbol{\lambda}_1^h, \boldsymbol{\lambda}_2^h\right) \in \mathbf{\Lambda}_1^h \times \mathbf{\Lambda}_2^h,
\end{aligned}
\tag{11}
$$

where the bilinear form $a(\mathbf{u},\mathbf{v})_\Omega$ and the inner product $(\mathbf{u},\mathbf{v})_\Omega$ are defined by

$$
\begin{aligned}
a(\mathbf{u},\mathbf{v})_\Omega &= \int_\Omega \left[(\nabla \times \mathbf{u}) \cdot \frac{1}{\mu_r}(\nabla \times \mathbf{v})\right] \mathrm{d}x^3 - k^2 \int_\Omega (\mathbf{u} \cdot \varepsilon_r \mathbf{v})\, \mathrm{d}x^3, \\
(\mathbf{u},\mathbf{v})_\Omega &= \int_\Omega (\mathbf{u} \cdot \mathbf{v})\, \mathrm{d}x^3, \\
(\mathbf{u},\mathbf{v})_{\partial\Omega} &= \int_{\partial\Omega} (\mathbf{u} \cdot \mathbf{v})\, \mathrm{d}x^2.
\end{aligned}
\tag{12}
$$

2.4. Fourier analysis of 1st order transmission conditions

In this section, a detailed analysis of the TCs used in the proposed DDM will be presented. As it was stated earlier, a proper choice of the TCs not only ensures uniqueness, but also accelerates the convergence of the DDM algorithm. Even though in practical DDM implementations TCs can be imposed on completely arbitrarily shaped interfaces, a general analysis of such situations can be very difficult. For that reason, we will restrict our analysis on planar interfaces only. Moreover, infinite lateral extent (half-space sub-domains) will be assumed, in order to facilitate the mathematical apparatus provided by the Fourier theory. A similar approach for the Maxwell's equations with another form of the TCs can be found in [36]. At this point, it should be noted that the Fourier analysis is restricted to rather idealistic geometries. However, it has been found that the convergence estimates provided by the analysis predict very accurately even for complicated interface boundaries, at least for two dimensional scalar Helmholtz problems [6].

For the reasons given, the simplified geometry of Fig. 5 will be considered. The electromagnetic boundary value problem of interest consists of the vector curl-curl equation of (1) in $\Omega = \mathbb{R}^3$, and the Silver-Muller radiation condition at infinity. Note that there is no PEC, PMC or material inhomogeneities ($\varepsilon_r(\mathbf{r}) = \mu_r(\mathbf{r}) = 1, \ \forall \mathbf{r} \in \Omega$) within Ω. The decomposed problem is that of (5) and (6) on $\Omega_1 = (-\infty, 0] \times \mathbb{R}^2$ and $\Omega_2 = [0, +\infty) \times \mathbb{R}^2$, respectively. Moreover, the interface is $\Gamma_{12} \equiv \Gamma = \mathbb{R}^2$, as shown in Fig. 5.

With respect to Fig. 5, let us first introduce the following two-dimensional Fourier transform pair:

$$
\begin{aligned}
\widehat{f}\,(k_x, k_y, z) &= \frac{1}{2\pi} \int_{-\infty}^{+\infty} \int_{-\infty}^{+\infty} f(x,y,z) \mathrm{e}^{\mathrm{j}\left(k_x x + k_y y\right)}\, \mathrm{d}x\, \mathrm{d}y, \\
f(x,y,z) &= \frac{1}{2\pi} \int_{-\infty}^{+\infty} \int_{-\infty}^{+\infty} \widehat{f}\,(k_x, k_y, z) \mathrm{e}^{-\mathrm{j}\left(k_x x + k_y y\right)}\, \mathrm{d}k_x\, \mathrm{d}k_y,
\end{aligned}
\tag{13}
$$

where $\widehat{f}$ denotes functions in Fourier domain, and k_x, k_y are the Fourier variables. In a straightforward way, the Fourier analysis of the "idealized" BVP will require the application of the Fourier transform

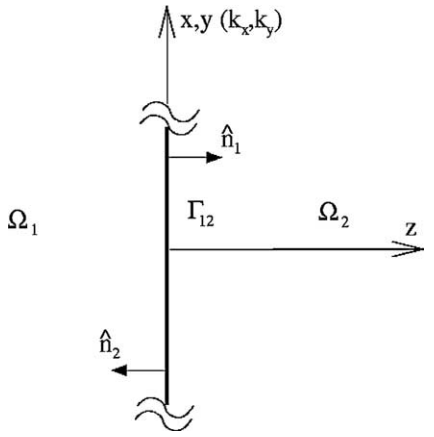

Fig. 5. Idealized domain decomposition model used in the Fourier analysis.

(13) on both vector curl-curl equation subject to the Silver–Muller radiation condition on each domain, and each of the TCs of (8) and (9). Even though this is a simple concept, the underling algebraic manipulations are very lengthy, and require analytic evaluations of the eigenvalues and eigenvectors of a 2×2 matrix, which leads to rather complicated final expressions for the convergence factors.

Rather than following that approach, we found it considerably easier to formulate the problem based on the concept of Transverse Electric (TE) or H and Transverse Magnetic (TM) or E modal decomposition of electromagnetic fields [30,31]. The electromagnetic fields produced by an arbitrary oriented electric or magnetic source in a "layered" environment, can be written as a superposition of TE and TM modes with respect to the "layered" interface normal [31]. The term "layered" implies geometry with multiple planar parallel interfaces that extend laterally at infinity. The problem of Fig. 5 belongs to the abovementioned category. In that case there is only one interface Γ_{12}. The other key ingredient of the following derivation is the use of rotation transformation of the Fourier variables k_x, k_y, which significantly simplifies the expressions of the electromagnetic fields in the Fourier domain.

For TE(H) modes [31]:

$$\begin{aligned}\mathbf{E} &= -\mathbf{z}\times\nabla\psi = \mathbf{x}\frac{\partial\psi}{\partial y} - \mathbf{y}\frac{\partial\psi}{\partial y},\\ \mathbf{H} &= -\frac{\eta}{\mathrm{j}k}(\nabla\times\nabla\times\mathbf{z}\psi) = -\frac{\eta}{\mathrm{j}k}\left[\mathbf{x}\frac{\partial^2\psi}{\partial x\,\partial z} + \mathbf{y}\frac{\partial^2\psi}{\partial y\,\partial z} - \mathbf{z}\left(\frac{\partial^2\psi}{\partial x^2}+\frac{\partial^2\psi}{\partial y^2}\right)\right].\end{aligned} \tag{14}$$

For TM(E) modes [31]:

$$\begin{aligned}\mathbf{E} &= \nabla\times\nabla\times\mathbf{z}\phi = \left[\mathbf{x}\frac{\partial^2\phi}{\partial x\,\partial z} + \mathbf{y}\frac{\partial^2\phi}{\partial y\,\partial z} - \mathbf{z}\left(\frac{\partial^2\phi}{\partial x^2}+\frac{\partial^2\phi}{\partial y^2}\right)\right],\\ \mathbf{H} &= -\frac{\mathrm{j}k}{\eta}(\mathbf{z}\times\nabla\phi) = -\frac{\mathrm{j}k}{\eta}\left(\mathbf{x}\frac{\partial\psi}{\partial y} - \mathbf{y}\frac{\partial\psi}{\partial x}\right),\end{aligned} \tag{15}$$

where ψ and ϕ satisfy

$$\left(\frac{\partial^2}{\partial x^2}+\frac{\partial^2}{\partial y^2}+\frac{\partial^2}{\partial z^2}+k^2\right)f(x,y,z) = 0, \quad f=\psi,\phi. \tag{16}$$

Taking the Fourier transform of (16) leads to

$$\left[\frac{\mathrm{d}^2}{\mathrm{d}z^2}+\left(k^2-\beta^2\right)\right]\widehat{f}\left(k_x,k_y,z\right)=0,\quad f=\psi,\phi, \tag{17}$$

where $\beta^2=k_x^2+k_y^2$ is the radial Fourier variable. In (17), it is convenient to further define the z-directed wave number as

$$k_z^2=\beta^2-k^2\ \Rightarrow\ k_z=\begin{cases}\mathrm{j}\sqrt{k^2-\beta^2} & k>|\beta|,\ \text{propagating modes}\\ \sqrt{\beta^2-k^2} & k<|\beta|,\ \text{evanescent modes}\end{cases} \tag{18}$$

Before applying the Fourier transform to (14) and (15), it would be useful to introduce the following transformation to the "natural" Fourier coordinate system $(k_x,k_y)\rightarrow(k_u,k_v)$. It will significantly simplify the field representations:

$$\begin{bmatrix}u\\ v\end{bmatrix}=\begin{bmatrix}\sin\alpha & -\cos\alpha\\ \cos\alpha & \sin\alpha\end{bmatrix}\begin{bmatrix}x\\ y\end{bmatrix}, \tag{19}$$

where the rotation angle is given by $\cos\alpha=k_x/\beta$ or $\sin\alpha=k_y/\beta$. Subsequently, we have

$$\begin{aligned}k_u&=k_x\sin\alpha-k_y\cos\alpha=0,\\ k_v&=k_x\cos\alpha+k_y\sin\alpha=\beta.\end{aligned} \tag{20}$$

We remark that the above-mentioned transformation can also be viewed as a transformation to the polar Fourier domain with the radial variable β, and the angular Fourier angle α. This is a fairly standard approach in dealing with the derivation of "layered" Green's functions in electromagnetics [32,33].

Having defined the auxiliary functions ψ and ϕ and the rotation transformation, it is time to apply the Fourier transform to the TE and TM modal fields of (14) and (15). In doing so, the following expressions are obtained for the TE modes:

$$\begin{aligned}\widehat{\mathbf{E}}&=-\mathrm{j}\left[\mathbf{x}k_y\widehat{\psi}-\mathbf{y}k_x\widehat{\psi}\right],\\ \widehat{\mathbf{H}}&=\frac{\eta}{\mathrm{j}k}\left[\mathbf{x}\mathrm{j}k_x\frac{\mathrm{d}\widehat{\psi}}{\mathrm{d}z}+\mathbf{y}\mathrm{j}k_y\frac{\mathrm{d}\widehat{\psi}}{\mathrm{d}z}-\mathbf{z}\beta^2\widehat{\psi}\right].\end{aligned} \tag{21}$$

Applying the rotation transformation of (19), the Fourier fields of the TE modes are further simplified to

$$\begin{aligned}\widehat{\mathbf{E}}&=-\mathbf{u}\mathrm{j}\beta\widehat{\psi},\\ \widehat{\mathbf{H}}&=\frac{\eta}{\mathrm{j}k}\left[\mathbf{v}\mathrm{j}\beta\frac{\mathrm{d}\widehat{\psi}}{\mathrm{d}z}-\mathbf{z}\beta^2\widehat{\psi}\right].\end{aligned} \tag{22}$$

Similarly, the TM Fourier fields in the rotated system are

$$\begin{aligned}\widehat{\mathbf{E}}&=-\mathbf{v}\mathrm{j}\beta\frac{\mathrm{d}\widehat{\phi}}{\mathrm{d}z}+\mathbf{z}\beta^2\widehat{\phi},\\ \widehat{\mathbf{H}}&=\mathbf{u}\frac{k}{\eta}\beta\widehat{\phi},\end{aligned} \tag{23}$$

where both $\widehat{\psi}$ and $\widehat{\phi}$ satisfy the homogeneous equation

$$\frac{\mathrm{d}\widehat{f}}{\mathrm{d}z}-k_z^2\widehat{f}=0,\quad f=\phi,\psi. \tag{24}$$

The general solutions of the ordinary differential equations in (24) are of the form

$$\widehat{f} = A^{+}\mathrm{e}^{-k_z z} + A^{-}\mathrm{e}^{+k_z z}. \tag{25}$$

Referring to the interface problem of Fig. 5 and subject to the Silver–Muller radiation condition on each appropriate sides of Ω_1 and Ω_2, becomes

$$\begin{aligned} \widehat{f}_1(k_x,k_y,z) &= F_1^{-}(k_x,k_y,0)\mathrm{e}^{k_z z} \quad \text{in } \Omega_1, \\ \widehat{f}_2(k_x,k_y,z) &= F_2^{+}(k_x,k_y,0)\mathrm{e}^{-k_z z} \quad \text{in } \Omega_2, \end{aligned} \tag{26}$$

where F_1^{-} and F_2^{+} are the Fourier modal excitation coefficients to be determined by the enforcement of the TC across the interface Γ_{12}. Note that the following part of the section, F_1^{-} and F_2^{+} will be replaced by A_1 and A_2, respectively, when referring to TM modes, and with B_1, B_2 when referring to TE modes. Putting together (22)–(24), the Fourier field representations of Table 1 are obtained.

The objective of this section is to find the convergence rates ρ^{TE} and ρ^{TM} for the TE and TM modes, respectively, as functions of k_z. To achieve that, it is necessary to find a relation between the excitation coefficients $A^{(n)}$ and $A^{(n-2)}$ for the TM modes, along with $B^{(n)}$ and $B^{(n-2)}$ for the TE modes, where the superscript $^{(n)}$ denotes the DD iteration number. This is done through the enforcement of TC on either domain, namely through the last equations of (8) and (9). Before doing that, it will be insightful to generalize the set of TC by assuming the Robin constant to be general complex number $\gamma \in \mathbb{C}$, rather than a purely imaginary number. We will denote this type of TCs as *Generalized Robin Transmission Conditions*. Through this modification, the Fourier transformed TCs in (8) and (9) become

$$\begin{aligned} \widehat{\mathbf{J}}_1^{(n)} - \gamma\widehat{\mathbf{e}}_1^{(n)} &= -\widehat{\mathbf{J}}_2^{(n-1)} - \gamma\widehat{\mathbf{e}}_2^{(n-1)} \quad \text{at } z = 0^{-}, \\ \widehat{\mathbf{J}}_2^{(n)} - \gamma\widehat{\mathbf{e}}_2^{(n)} &= -\widehat{\mathbf{J}}_1^{(n-1)} - \gamma\widehat{\mathbf{e}}_1^{(n-1)} \quad \text{at } z = 0^{+}. \end{aligned} \tag{27}$$

The analysis proceeds by finding $\widehat{\mathbf{J}}_i$ and $\widehat{\mathbf{e}}_i$, $i = 1,2$ with the use of Table 1. After some very simple and short algebraic manipulations, the tangential Fourier fields of Table 2 are obtained. Note that with the use of the rotation transformation in the Fourier domain, the tangential TE and TM fields are completely decoupled. This is reflected on Table 2, where the TE representation involves only **u** coordinate whereas the TM representation involves **v** coordinate only.

Table 1
TE and TM Fourier field representations on the two subdomains

	Ω_1		Ω_2	
	$\widehat{\mathbf{E}}^{(n)}$	$\widehat{\mathbf{H}}^{(n)}$	$\widehat{\mathbf{E}}^{(n)}$	$\widehat{\mathbf{H}}^{(n)}$
TE	$-B_1^{(n)}\mathrm{j}\beta\mathrm{e}^{+k_z z}\mathbf{u}$	$B_1^{(n)}\frac{\eta}{\mathrm{j}k}(\mathbf{v}\mathrm{j}k_z - \mathbf{z}\beta)\beta\mathrm{e}^{+k_z z}$	$-B_2^{(n)}\mathrm{j}\beta\mathrm{e}^{-k_z z}\mathbf{u}$	$-B_2^{(n)}\frac{\eta}{\mathrm{j}k}(\mathbf{v}\mathrm{j}k_z + \mathbf{z}\beta)\beta\mathrm{e}^{-k_z z}$
TM	$A_1^{(n)}(-\mathbf{v}\mathrm{j}k_z + \mathbf{z}\beta)\beta\mathrm{e}^{+k_z z}$	$A_1^{(n)}\frac{k}{\eta}\beta\mathrm{e}^{+k_z z}\mathbf{u}$	$A_2^{(n)}(\mathbf{v}\mathrm{j}k_z + \mathbf{z}\beta)\beta\mathrm{e}^{-k_z z}$	$A_2^{(n)}\frac{k}{\eta}\beta\mathrm{e}^{-k_z z}\mathbf{u}$

Table 2
TE and TM Fourier tangential field representations on the domain interface

	Ω_1		Ω_2	
	$\widehat{\mathbf{e}}^{(n)}(z=0^{-})$	$\widehat{\mathbf{J}}^{(n)}(z=0^{-})$	$\widehat{\mathbf{e}}^{(n)}(z=0^{+})$	$\widehat{\mathbf{J}}^{(n)}(z=0^{+})$
TE	$-B_1^{(n)}\mathrm{j}\beta\mathbf{u}$	$B_1^{(n)}\mathrm{j}\beta k_z\mathbf{u}$	$-B_2^{(n)}\mathrm{j}\beta\mathbf{u}$	$B_2^{(n)}\mathrm{j}\beta k_z\mathbf{u}$
TM	$-A_1^{(n)}\mathrm{j}k_z\beta\mathbf{v}$	$-A_1^{(n)}\mathrm{j}k^2\beta\mathbf{v}$	$A_2^{(n)}\mathrm{j}k_z\beta\mathbf{v}$	$A_2^{(n)}\mathrm{j}k^2\beta\mathbf{v}$

With this observation in mind it is now straightforward to substitute the values of Table 2 on (27) and obtain the following convergence factors

$$\rho^{\mathrm{TE}}(k_z) = \frac{\left|B_1^{(n)}\right|}{\left|B_1^{(n-2)}\right|} = \left|\frac{k_z - \gamma}{k_z + \gamma}\right|^2, \tag{28}$$

for the TE modes; and,

$$\rho^{\mathrm{TM}}(k_z) = \frac{\left|A_1^{(n)}\right|}{\left|A_1^{(n-2)}\right|} = \left|\frac{k^2 + \gamma k_z}{k^2 - \gamma k_z}\right|^2 \tag{29}$$

for the TM modes. In a more convenient way, the convergence estimates of (28) and (29), can be written in terms of the transverse spectral variable β, with the aid of (18). Consequently, we have

$$\rho^{\mathrm{TE}}(\beta) = \begin{cases} \left|\frac{\mathrm{j}\sqrt{k^2-\beta^2}-\gamma}{\mathrm{j}\sqrt{k^2-\beta^2}+\gamma}\right|^2, & k > |\beta|, \text{ propagating modes,} \\ \left|\frac{\sqrt{\beta^2-k^2}-\gamma}{\sqrt{\beta^2-k^2}+\gamma}\right|^2, & k < |\beta|, \text{ evanescent modes} \end{cases} \tag{30}$$

and

$$\rho^{\mathrm{TM}}(\beta) = \begin{cases} \left|\frac{k^2+\mathrm{j}\gamma\sqrt{k^2-\beta^2}}{k^2+\mathrm{j}\gamma\sqrt{k^2-\beta^2}}\right|^2, & k > |\beta|, \text{ propagating modes,} \\ \left|\frac{k^2+\gamma\sqrt{\beta^2-k^2}}{k^2+\gamma\sqrt{\beta^2-k^2}}\right|^2, & k < |\beta|, \text{ evanescent modes.} \end{cases} \tag{31}$$

In a convergent DD scheme that employs a stationary outer loop iteration, all four modes in (30) and (31) should have $\rho < 1$. This implies that our analysis and convergence rates are valid for both Jacobi and Gauss–Seidel iteration schemes, or in terms of the Schwarz theory, both additive and multiplicative Schwarz. On the other hand, if each of the above schemes is used as a preconditioner accelerator on a Krylov type method, a spectral radius $\rho > 1$ does not necessarily imply that the method diverges.

In light of (30), (31) and the comments made, a number of convergent regions can be identified for each set of modes, based on the choice of the Robin constant γ. From (30), it is clear that choosing $\mathrm{Im}\{\gamma\} > 0$ will lead to convergent TE propagation modes, whereas the $\mathrm{Re}\{\gamma\} > 0$ would lead to convergent TE evanescent modes. These convergent regions for the TE modes are depicted at Fig. 6(a) in the complex γ-plane. It is clear that the first quadrant will be the choice of preference since both evanescent and propagation modes converge. This is exactly the case described in [6] for the two-dimensional Helmholtz equation. Furthermore, like the Helmholtz case, even if γ is chosen on the appropriate quadrant, the cut-off mode $\beta = k$ (plane-wave incidence parallel to the interface) will never converge, since that choice makes $\rho^{\mathrm{TE}}(\beta = k) = 1$. On the other hand, the situation for the TM modes is quite different. From (31), the propagating TM modes will converge in the region where $\mathrm{Im}\{\gamma\} > 0$, but the evanescent ones will converge on the region $\mathrm{Re}\{\gamma\} < 0$, which is complementary to the evanescent TE modes case. Again the regions of convergence for the TM modes are plotted in the complex γ-plane in Fig. 6(b). This is a situation unique to the Maxwell equations. Unfortunately, this complicates the convergence behavior of a stationary iteration DDM. As it is apparent from Fig. 6, there is no region where all four modes are convergent. In the first quadrant, all TE modes together with the propagating TM modes are convergent, but the evanescent TM modes are divergent $\rho^{\mathrm{TM}}_{\mathrm{evan}} >$

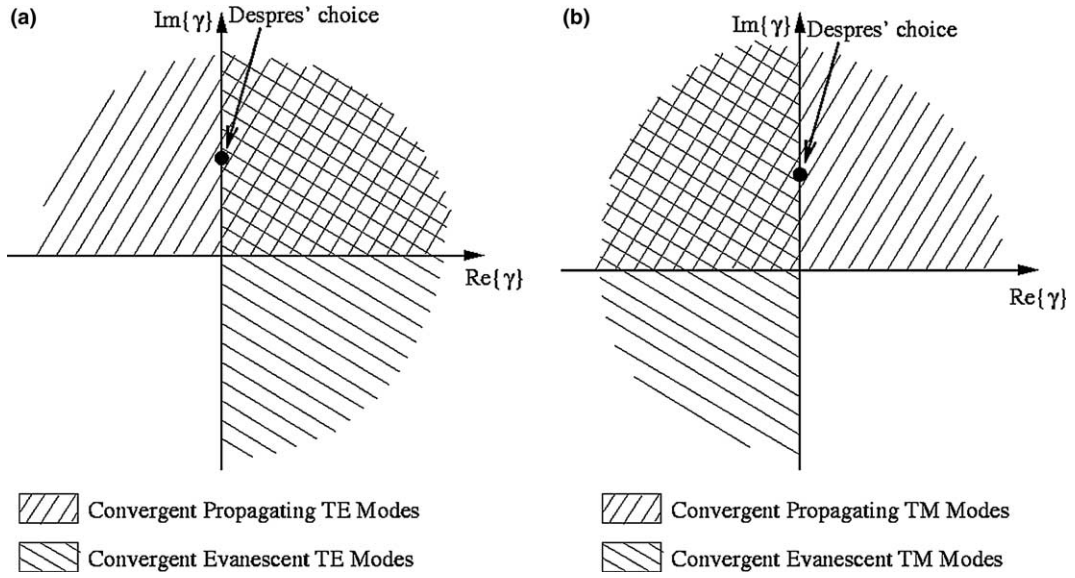

Fig. 6. Regions of convergence for propagating and evanescent: (a) TE modes and (b) TM modes.

Fortunately, for the radiating problems, such as the antenna arrays, the evanescent modes along one particular interface will be the propagating modes along other interfaces. Therefore, the choice where all the propagating modes converge and $\rho_{\text{evan}}^{\text{TE}} = \rho_{\text{evan}}^{\text{TM}} = 1$ will be sufficient to provide a convergent DDM. Such a choice was provided by Després et al. in their original paper [14]. In that work $\gamma = \mathrm{j}k$ was used; this choice is also depicted in Fig. 6. Throughout this paper, the same γ has been used.

2.5. DDM as a preconditioner

In this section, we shall reformulate our DDM in a slightly different way and show that the DDM method proposed herein can be viewed as a preconditioner. We start by rewriting the BVP in $\Omega^h = \Omega_1^h \cup \Omega_2^h$ (we shall omit the superscript ^{h} whenever it is obvious) and employing the auxiliary variables $\mathbf{J}_1$ and $\mathbf{J}_2$:

$$
\begin{aligned}
&\nabla \times \frac{1}{\mu_r} \nabla \times \mathbf{E}_1 - k^2 \varepsilon_r \mathbf{E}_1 = -\mathrm{j}\omega\mu_0 \mathbf{J}_1^{\text{imp}} \quad \text{in } \Omega_1,\\
&\nabla \times \frac{1}{\mu_r} \nabla \times \mathbf{E}_2 - k^2 \varepsilon_r \mathbf{E}_2 = -\mathrm{j}\omega\mu_0 \mathbf{J}_2^{\text{imp}} \quad \text{in } \Omega_2,\\
&\gamma_{\mathrm{t}}(\mathbf{E}_1) = \gamma_{\mathrm{t}}(\mathbf{E}_2) = 0 \quad \text{on } \Gamma_{\text{pec}},\\
&\gamma_{\mathrm{t}}^{\times}\left(\frac{1}{\mu_r}\nabla \times \mathbf{E}_1\right) = \gamma_{\mathrm{t}}^{\times}\left(\frac{1}{\mu_r}\nabla \times \mathbf{E}_2\right) = 0 \quad \text{on } \Gamma_{\text{pmc}},\\
&\gamma_{\mathrm{t}}^{\times}\left(\frac{1}{\mu_r}\nabla \times \mathbf{E}_1\right) - \mathrm{j}k\gamma_{\mathrm{t}}(\mathbf{E}_1) = \gamma_{\mathrm{t}}^{\times}\left(\frac{1}{\mu_r}\nabla \times \mathbf{E}_2\right) - \mathrm{j}k\gamma_{\mathrm{t}}(\mathbf{E}_2) = 0 \quad \text{on } \Gamma_{\infty},\\
&\mathbf{J}_1 = \gamma_{\mathrm{t}}^{\times}\left(\frac{1}{\mu_r}\nabla \times \mathbf{E}_1\right)_{\Gamma_1}, \quad \mathbf{J}_2 = \gamma_{\mathrm{t}}^{\times}\left(\frac{1}{\mu_r}\nabla \times \mathbf{E}_2\right)_{\Gamma_2},\\
&\mathbf{J}_1 - \mathrm{j}k\mathbf{e}_1 = -\mathbf{J}_2 - \mathrm{j}k\mathbf{e}_2 \quad \text{on } \Gamma_1,\\
&\mathbf{J}_2 - \mathrm{j}k\mathbf{e}_2 = -\mathbf{J}_1 - \mathrm{j}k\mathbf{e}_1 \quad \text{on } \Gamma_2.
\end{aligned}
\tag{32}
$$

Subsequently, the corresponding Galerkin formulation can be stated as

$$\begin{aligned}
&\text{Seek } (\mathbf{E}_1,\mathbf{E}_2)\in \mathbf{S}_1\times\mathbf{S}_2 \text{ and } (\mathbf{J}_1,\mathbf{J}_2)\in \mathbf{\Lambda}_1\times\mathbf{\Lambda}_2 \text{ such that}\\
&a(\mathbf{v}_1,\mathbf{E}_1)_{\Omega_1}+a(\mathbf{v}_2,\mathbf{E}_2)_{\Omega_2}+\mathrm{j}k(\gamma_{\mathrm{t}}\mathbf{v}_1,\mathbf{e}_1)_{\partial\Omega_1\cap\Gamma_\infty}+\mathrm{j}k(\gamma_{\mathrm{t}}\mathbf{v}_2,\mathbf{e}_2)_{\partial\Omega_2\cap\Gamma_\infty}+(\gamma_{\mathrm{t}}\mathbf{v}_1,\mathbf{J}_1)_{\Gamma_1}+(\gamma_{\mathrm{t}}\mathbf{v}_2,\mathbf{J}_2)_{\Gamma_2}\\
&\quad=\frac{-\mathrm{j}k}{\eta}\left(\mathbf{v}_1,\mathbf{J}_1^{\mathrm{imp}}\right)_{\Omega_1}-\frac{\mathrm{j}k}{\eta}\left(\mathbf{v}_2,\mathbf{J}_2^{\mathrm{imp}}\right)_{\Omega_2},\\
&(\boldsymbol{\lambda}_1,\mathbf{e}_1)_{\Gamma_1}+\frac{\mathrm{j}}{k}(\boldsymbol{\lambda}_1,\mathbf{J}_1)_{\Gamma_1}-(\boldsymbol{\lambda}_1,\mathbf{e}_2)_{\Gamma_1}+\frac{\mathrm{j}}{k}(\boldsymbol{\lambda}_1,\mathbf{J}_2)_{\Gamma_1}=0,\\
&(\boldsymbol{\lambda}_2,\mathbf{e}_2)_{\Gamma_2}+\frac{\mathrm{j}}{k}(\boldsymbol{\lambda}_2,\mathbf{J}_2)_{\Gamma_2}-(\boldsymbol{\lambda}_2,\mathbf{e}_1)_{\Gamma_2}+\frac{\mathrm{j}}{k}(\boldsymbol{\lambda}_2,\mathbf{J}_1)_{\Gamma_2}=0,\\
&\forall(\mathbf{v}_1,\mathbf{v}_2)\in\mathbf{S}_1\times\mathbf{S}_2 \text{ and } (\boldsymbol{\lambda}_1,\boldsymbol{\lambda}_2)\in\mathbf{\Lambda}_1\times\mathbf{\Lambda}_2.
\end{aligned}\tag{33}$$

Let us introduce a notation here to facilitate our discussion. For a vector $\mathbf{u}\in\mathbf{S}_1\times\mathbf{S}_2\times\mathbf{\Lambda}_1\times\mathbf{\Lambda}_2$, we can express it as

$$\mathbf{u}=\begin{bmatrix}\mathbf{u}_1\\ \mathbf{u}_2\\ \mathbf{J}_1^{(\mathbf{u})}\\ \mathbf{J}_2^{(\mathbf{u})}\end{bmatrix}=\begin{bmatrix}\underset{\sim}{\mathbf{W}}_1 & 0 & 0 & 0\\ 0 & \underset{\sim}{\mathbf{W}}_2 & 0 & 0\\ 0 & 0 & \underset{\sim}{\mathbf{W}}_1 & 0\\ 0 & 0 & 0 & \underset{\sim}{\mathbf{W}}_2\end{bmatrix}\begin{bmatrix}\tilde{\mathbf{u}}_1\\ \tilde{\mathbf{u}}_2\\ \tilde{\mathbf{J}}_1^{(\mathbf{u})}\\ \tilde{\mathbf{J}}_2^{(\mathbf{u})}\end{bmatrix},\tag{34}$$

where the symbol $\square$ means a row vector and $\underset{\sim}{\square}$ indicates a column vector. Also, in Eq. (34), the entries in the row vector $\underset{\sim}{\mathbf{W}}$ span the finite dimensional subspace $\mathbf{S}_i\subset\mathbf{H}_0(\mathrm{curl};\Omega_i)$. Similarly, we have the entries in $\underset{\sim}{\boldsymbol{\alpha}}$ span the subspace $\mathbf{\Lambda}_i\subset\mathbf{H}_{\|}^{-1/2}(\mathrm{div}_\Gamma;\Gamma_i)$. The column vectors $\tilde{\mathbf{u}}_1$ and $\tilde{\mathbf{u}}_2$ are the coefficient vectors of $\mathbf{u}_1$ and $\mathbf{u}_2$, respectively. Similar definitions are for the column vectors $\tilde{\mathbf{J}}_1^{(\mathbf{u})}$ and $\tilde{\mathbf{J}}_2^{(\mathbf{u})}$. We further partition the coefficient vector $\tilde{\mathbf{u}}_i$ into two sub-column vectors, that is

$$\tilde{\mathbf{u}}_i=\begin{bmatrix}\tilde{\mathbf{u}}_i^I\\ \tilde{\mathbf{u}}_i^\Gamma\end{bmatrix}\tag{35}$$

with $\tilde{\mathbf{u}}_i^I$ refers to the coefficients inside sub-domain Ω_i and $\tilde{\mathbf{u}}_i^\Gamma$ for the coefficients on the boundary Γ_i. Consequently, it can be shown that the final matrix equation for the Galerkin formulation (33) is

$$\begin{bmatrix}\mathbf{A_1} & \mathbf{C_1} & \mathbf{0} & \mathbf{0} & \mathbf{0} & \mathbf{0}\\ \mathbf{C_1^T} & \mathbf{B_1} & \mathbf{D_1} & \mathbf{0} & \mathbf{0} & \mathbf{0}\\ \mathbf{0} & \mathbf{D_1^t} & \frac{\mathrm{j}}{k}\mathbf{T_1} & \mathbf{0} & -\mathbf{D_{12}^t} & \frac{\mathrm{j}}{k}\mathbf{T_{12}}\\ \mathbf{0} & \mathbf{0} & \mathbf{0} & \mathbf{A_2} & \mathbf{C_2} & \mathbf{0}\\ \mathbf{0} & \mathbf{0} & \mathbf{0} & \mathbf{C_2^t} & \mathbf{B_2} & \mathbf{D_2}\\ \mathbf{0} & -\mathbf{D_{21}^t} & \frac{\mathrm{j}}{k}\mathbf{T_{21}} & \mathbf{0} & \mathbf{D_2^t} & \frac{\mathrm{j}}{k}\mathbf{T_2}\end{bmatrix}\begin{bmatrix}\tilde{\mathbf{u}}_1^I\\ \tilde{\mathbf{u}}_1^\Gamma\\ \tilde{\mathbf{J}}_1^{(\mathbf{u})}\\ \tilde{\mathbf{u}}_2^I\\ \tilde{\mathbf{u}}_2^\Gamma\\ \tilde{\mathbf{J}}_2^{(\mathbf{u})}\end{bmatrix}=\begin{bmatrix}\tilde{\mathbf{y}}_1\\ 0\\ 0\\ \tilde{\mathbf{y}}_2\\ 0\\ 0\end{bmatrix},\tag{36}$$

where the matrix entries are defined such that $\forall\mathbf{v}=[\,\mathbf{v}_1\quad\mathbf{v}_2\quad\mathbf{J}_1^{(\mathbf{v})}\quad\mathbf{J}_2^{(\mathbf{v})}\,]^{\mathrm{t}}\in\mathbf{S}_1\times\mathbf{S}_2\times\mathbf{\Lambda}_1\times\mathbf{\Lambda}_2$, we have

$$\begin{aligned}
&\begin{bmatrix}\tilde{\mathbf{v}}_i^I & \tilde{\mathbf{v}}_i^\Gamma\end{bmatrix}\begin{bmatrix}\mathbf{A}_i & \mathbf{C}_i & 0\\ \mathbf{C}_i^t & \mathbf{B}_i & \mathbf{D}_i\end{bmatrix}\begin{bmatrix}\tilde{\mathbf{u}}_i^I\\ \tilde{\mathbf{u}}_i^\Gamma\\ \tilde{\mathbf{J}}_i^{(\mathbf{u})}\end{bmatrix}=a(\mathbf{v}_i,\mathbf{u}_i)_{\Omega_i}+\mathrm{j}k(\gamma_{\mathrm{t}}\mathbf{v}_i,\mathbf{u}_i)_{\partial\Omega_i\cap\Gamma_\infty}+\left(\gamma_{\mathrm{t}}\mathbf{v}_i,\mathbf{J}_i^{(\mathbf{u})}\right)_{\Gamma_i},\\
&\underset{\sim i}{\mathbf{J}}^{(\mathbf{v})}\mathbf{D}_{ij}^t\tilde{\mathbf{u}}_j^\Gamma=\left(\mathbf{J}_i^{(\mathbf{v})},\gamma_{\mathrm{t}}\mathbf{u}_j\right)_{\Gamma_i},\quad\underset{\sim i}{\mathbf{J}}^{(\mathbf{v})}\mathbf{T}_i\tilde{\mathbf{J}}_i^{(\mathbf{u})}=\left(\mathbf{J}_i^{(\mathbf{v})},\mathbf{J}_i^{(\mathbf{u})}\right)_{\Gamma_i},\quad\underset{\sim i}{\mathbf{J}}^{(\mathbf{v})}\mathbf{T}_{ij}\tilde{\mathbf{J}}_j^{(\mathbf{u})}=\left(\mathbf{J}_i^{(\mathbf{v})},\mathbf{J}_j^{(\mathbf{u})}\right)_{\Gamma_i}.
\end{aligned}\tag{37}$$

The formulation introduced in Eq. (11) can now be solved through

$$\begin{bmatrix} \mathbf{A_1} & \mathbf{C_1} & \mathbf{0} & \mathbf{0} & \mathbf{0} & \mathbf{0} \\ \mathbf{C_1^T} & \mathbf{B_1} & \mathbf{D_1} & \mathbf{0} & \mathbf{0} & \mathbf{0} \\ \mathbf{0} & \mathbf{D_1^t} & \frac{\mathrm{j}}{k}\mathbf{T_1} & \mathbf{0} & \mathbf{0} & \mathbf{0} \\ \mathbf{0} & \mathbf{0} & \mathbf{0} & \mathbf{A_2} & \mathbf{C_2} & \mathbf{0} \\ \mathbf{0} & \mathbf{0} & \mathbf{0} & \mathbf{C_2^t} & \mathbf{B_2} & \mathbf{D_2} \\ \mathbf{0} & \mathbf{0} & \mathbf{0} & \mathbf{0} & \mathbf{D_2^t} & \frac{\mathrm{j}}{k}\mathbf{T_2} \end{bmatrix} \begin{bmatrix} \tilde{\mathbf{u}}_1^I \\ \tilde{\mathbf{u}}_1^\Gamma \\ \tilde{\mathbf{J}}_1^{(\mathbf{u})} \\ \tilde{\mathbf{u}}_2^I \\ \tilde{\mathbf{u}}_2^\Gamma \\ \tilde{\mathbf{J}}_2^{(\mathbf{u})} \end{bmatrix}^{(n+1)} = \begin{bmatrix} \tilde{\mathbf{y}}_1 \\ 0 \\ 0 \\ \tilde{\mathbf{y}}_2 \\ 0 \\ 0 \end{bmatrix} + \begin{bmatrix} \mathbf{0} & \mathbf{0} & \mathbf{0} & \mathbf{0} & \mathbf{0} & \mathbf{0} \\ \mathbf{0} & \mathbf{0} & \mathbf{0} & \mathbf{0} & \mathbf{0} & \mathbf{0} \\ \mathbf{0} & \mathbf{0} & \mathbf{0} & \mathbf{0} & \mathbf{D_{12}^t} & -\frac{\mathrm{j}}{k}\mathbf{T_{12}} \\ \mathbf{0} & \mathbf{0} & \mathbf{0} & \mathbf{0} & \mathbf{0} & \mathbf{0} \\ \mathbf{0} & \mathbf{0} & \mathbf{0} & \mathbf{0} & \mathbf{0} & \mathbf{0} \\ \mathbf{0} & \mathbf{D_{21}^t} & -\frac{\mathrm{j}}{k}\mathbf{T_{21}} & \mathbf{0} & \mathbf{0} & \mathbf{0} \end{bmatrix} \begin{bmatrix} \tilde{\mathbf{u}}_1^I \\ \tilde{\mathbf{u}}_1^\Gamma \\ \tilde{\mathbf{J}}_1^{(\mathbf{u})} \\ \tilde{\mathbf{u}}_2^I \\ \tilde{\mathbf{u}}_2^\Gamma \\ \tilde{\mathbf{J}}_2^{(\mathbf{u})} \end{bmatrix}^{(n)}, \tag{38}$$

where $[]^{(n)}$ indicates the solution at the nth iteration. Obviously, Eq. (38) can be solved by a more efficient Gauss–Seidel iteration where the iteration is always updated through the most *recent* unknown values. However, as pointed out in the previous section, fixed point algorithms such as Jacobi and Gauss–Seidel methods will not damp the evanescent modes. This is not a serious restriction in the present paper since radiating applications are of primary interest in this paper. Nevertheless, relaxation on the interface [13,14] or Krylov methods [6] can be considered to improve the convergence of the algorithm.

To take advantage of the periodicity of the current large finite antenna array applications, we utilize the fact

$$\begin{bmatrix} \mathbf{A_1} & \mathbf{C_1} & \mathbf{0} \\ \mathbf{C_1^t} & \mathbf{B_1} & \mathbf{D_1} \\ \mathbf{0} & \mathbf{D_1^t} & \frac{\mathrm{j}}{k}\mathbf{T_1} \end{bmatrix} = \begin{bmatrix} \mathbf{A_2} & \mathbf{C_2} & \mathbf{0} \\ \mathbf{C_2^t} & \mathbf{B_2} & \mathbf{D_2} \\ \mathbf{0} & \mathbf{D_2^t} & \frac{\mathrm{j}}{k}\mathbf{T_2} \end{bmatrix}. \tag{39}$$

Subsequently, for each iteration, we shall only need to solve

$$\begin{bmatrix} \mathbf{A_1} & \mathbf{C_1} & \mathbf{0} \\ \mathbf{C_1^t} & \mathbf{B_1} & \mathbf{D_1} \\ \mathbf{0} & \mathbf{D_1^t} & \frac{\mathrm{j}}{k}\mathbf{T_1} \end{bmatrix} \begin{bmatrix} \tilde{\mathbf{u}}_i^I \\ \tilde{\mathbf{u}}_i^\Gamma \\ \tilde{\mathbf{J}}_i^{(\mathbf{u})} \end{bmatrix}^{(n+1)} = \begin{bmatrix} \tilde{\mathbf{y}}_i \\ \mathbf{0} \\ \mathbf{0} \end{bmatrix} + \begin{bmatrix} \mathbf{0} & \mathbf{0} & \mathbf{0} \\ \mathbf{0} & \mathbf{0} & \mathbf{0} \\ \mathbf{0} & \mathbf{D_{ij}^t} & -\frac{\mathrm{j}}{k}\mathbf{T_{ij}} \end{bmatrix} \begin{bmatrix} \tilde{\mathbf{u}}_j^I \\ \tilde{\mathbf{u}}_j^\Gamma \\ \tilde{\mathbf{J}}_j^{(\mathbf{u})} \end{bmatrix}^{(n)}, \quad i = 1,2; \;\; j = \{1,2\}/i. \tag{40}$$

3. Numerical results

We first validate the proposed approach by solving a few exponentially tapered notch (Vivaldi) antenna arrays and comparing the results with other methods. Hereafter, the exponentially tapered notch antenna is denoted as Vivaldi antenna for simplicity. The precise dimensions of a single Vivaldi antenna element are shown in Fig. 7. For small size arrays, the results obtained by the current DDM are compared to those computed through direct finite element/boundary integral (FEBI) method [34]. The array configurations used in this section have been previously analyzed in [35] using the FDTD method. All the arrays analyzed herein have a Vivaldi element as the basic building block. Details of the array configurations can be found in [35]. All arrays are operated at frequency $f = 5.0$ GHz, under a uniform broadside excitation. The whole array structure is backed by a finite PEC ground plane, which is placed 10 mm behind the Vivaldi elements. The single antenna block was initially discretized by higher order ($p = 2$) tetrahedral elements with average mesh size of $\lambda/3$, where λ is the wavelength in the free space. The mesh was further refined by h-adaptive mesh refinement scheme presented in [27].

For all results the (far-field) antenna pattern of each array is presented. Notice that the antenna pattern is usually the most important figure-of-merit of an antenna. The antenna pattern of each antenna array was

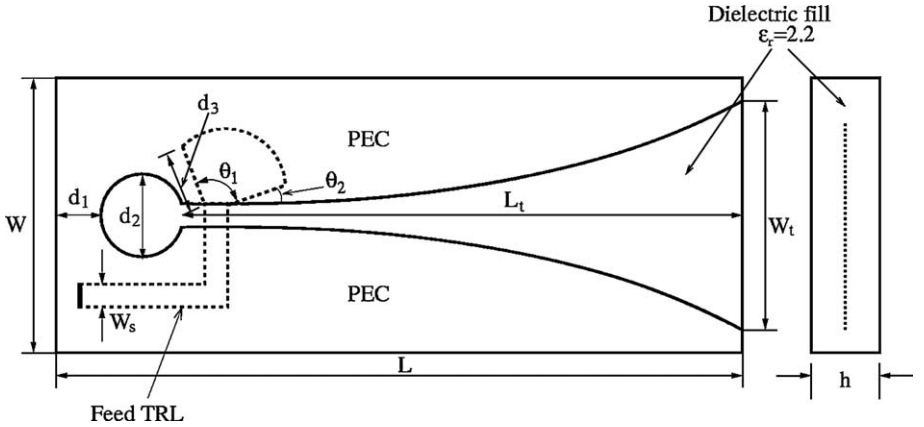

Fig. 7. Geometry, dimension and material parameters of a single Vivaldi array elements: $L = 81.6$ mm, $W = 25.6$ mm, $L_t = 61.6$ mm, $W_t = 24.0$ mm, $W_s = 8.8$ mm, h = 8.8 mm, $d_1 = 5.6$ mm, $d_2 = 8.8$ mm, $d_3 = 9.6$ mm, $\theta_1 = 100°$, and $\theta_2 = 25°$.

calculated through a near-to-far field transformation based on Huygen's principle. Namely, the electric field at $r \to \infty$ can be obtained by [1]

$$\mathbf{E}(\mathbf{r}) = \frac{e^{-jkr}}{4\pi r} \int_{\partial\Omega} \{j\omega\mu\hat{\mathbf{r}} \times [\hat{\mathbf{r}} \times \mathbf{J}(\mathbf{r}')] + jk\hat{\mathbf{r}} \times \mathbf{M}(\mathbf{r}')\} e^{jk\hat{\mathbf{r}}\mathbf{r}'} \, dx'^2, \tag{41}$$

where $\partial\Omega$ is the truncation surface enclosing entire array, $\mathbf{r}$ the observation point, and $\mathbf{r}'$ the point on the near-field surface $\partial\Omega$. The electric and magnetic current densities, $\mathbf{J}(\mathbf{r}')$ and $\mathbf{M}(\mathbf{r}')$, are found by

$$\begin{aligned} \mathbf{J}(\mathbf{r}') &= \sum_i u_i(\mathbf{n} \times \nabla \times \mathbf{W}_i(\mathbf{r}')), \\ \mathbf{M}(\mathbf{r}') &= \sum_i u_i(\mathbf{W}_i(\mathbf{r}') \times \mathbf{n}), \end{aligned} \tag{42}$$

where i spans the truncation surface $\partial\Omega$ unknowns only, and $\mathbf{n}$ is a unit vector normal to the surface $\partial\Omega$ pointing away from Ω. u_i is the ith solution coefficient introduced in (34), furthermore, $\mathbf{W}_i$ is the basis function for u_i. Using (41), the antenna pattern is defined as

$$\text{Antenna Pattern } [\text{dB}] = 10 \log \frac{|\mathbf{E}(\mathbf{r})|^2}{\max\left[|\mathbf{E}(\mathbf{r})|^2\right]}. \tag{43}$$

The antenna patterns calculated by both DDM and FEBI for the 3×3 and 7×7 Vivaldi arrays were compared in Figs. 8 and 10. In both cases the DDM results agree favorably with the reference FEBI answers over the entire angular spectrum. For DDM simulations, only one Vivaldi element was created and repeatedly used for other elements. Therefore, the main memory consumption for DDM takes place in the storage of the matrix equation for only one Vivaldi element and one unknown vector for each sub-domain assuming Gauss–Seidel iteration scheme. In the solution procedure, the relative residual was defined as

$$\text{resid} = \max\left(\frac{\left\|\mathbf{u}_i^{(n)} - \mathbf{u}_i^{(n-1)}\right\|_\infty}{\left\|\mathbf{u}_i^{(n)}\right\|_\infty}\right), \tag{44}$$

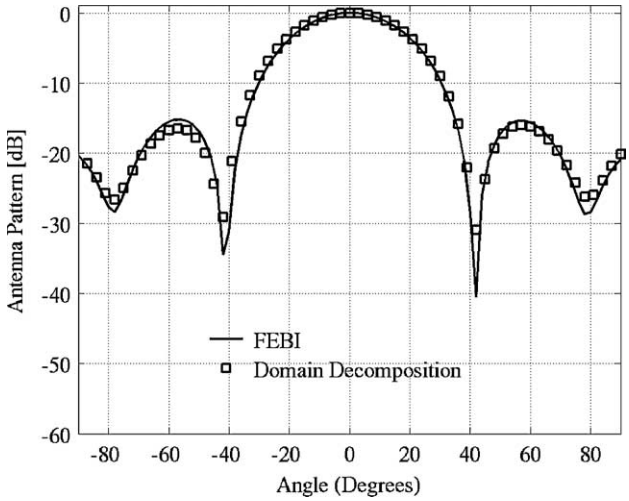

Fig. 8. E-plane antenna pattern of a 3×3 Vivaldi antenna array.

where $\mathbf{u}_i^{(n)}$ is the solution vector for the ith sub-domain at the nth iteration, and $\|\cdot\|_\infty$ the infinite norm of a vector. The iteration started from an initial guess of $\mathbf{u}_i^{(0)} = \mathbf{0}$ for each sub-domain Ω_i. It terminated once the residual defined by (44) was smaller than the tolerance. We have used tolerance of 10^{-1}, and through various numerical experiments, we found that this is sufficient for obtaining accurate antenna patterns.

To observe the improved convergence of the Gauss–Seidel over Jacobi method, the 3×3 Vivaldi array example was solved by both methods and the comparison is presented in Fig. 9. The convergence curves certainly indicate much improved convergence with Gauss–Seidel. It is noted that, theoretically the Gauss–Seidel scheme should converge twice faster than Jacobi method [4]. In addition, Gauss–Seidel procedure requires only one unknown vector per iteration, whereas Jacobi stores the present and the previous solution vectors per iteration. Another interesting phenomenon can be observed in Fig. 11, where the antenna patterns of the 7×7 array are plotted for 1st, 5th, 10th and 28th iterations. Note that the 28th

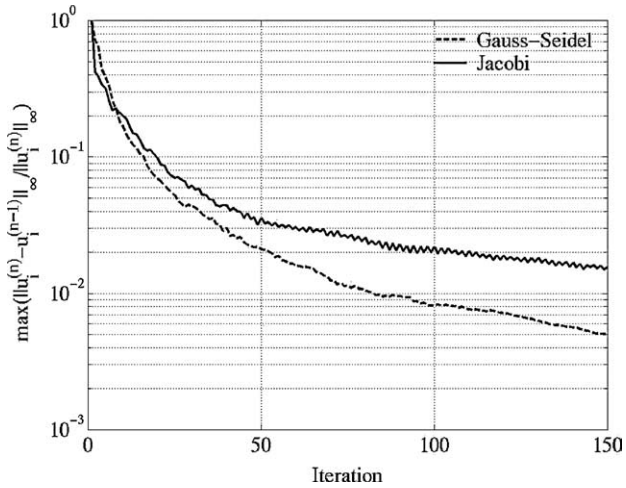

Fig. 9. Convergence of Jacobi and Gauss–Seidel outer-loop iterations of DDM for 3×3 Vivaldi antenna array.

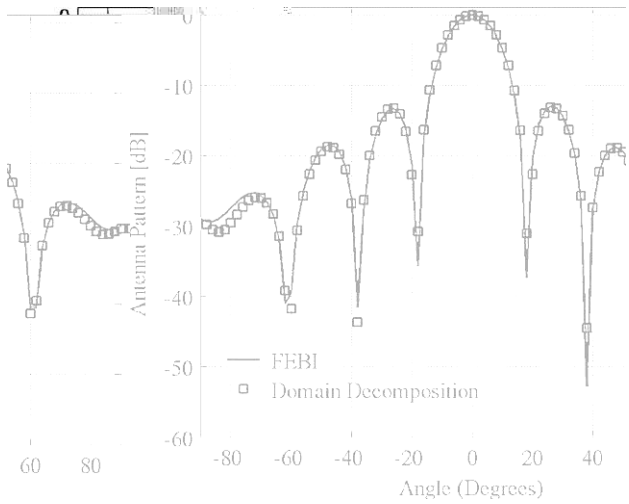

Fig. 10. E-plane antenna pattern of a 7×7 Vivaldi antenna array.

iteration is already converged; the pattern is practically unchanged for higher number of iterations. In this case Jacobi method was purposely used to observe the effect of the coupling between elements. In the Jacobi method, the first iteration does not calculate the interaction between elements, therefore, the array factor of the array can be observed. As the iteration proceeds, the field excited by an antenna element propagates farther away. Consequently, Fig. 11 shows how the antenna pattern converges as more coupling between antenna elements is taken into account.

We then apply the DDM to large finite arrays. One of the important advantages of DDM is that large periodic structures can be solved on a common PC. For a periodic structure, the matrix equation for a single block can be repeatedly used for all other blocks in the DDM procedure. As a result, the memory requirement for the matrix equation is insignificant. The antenna patterns of 50×50 and 100×100 ele-

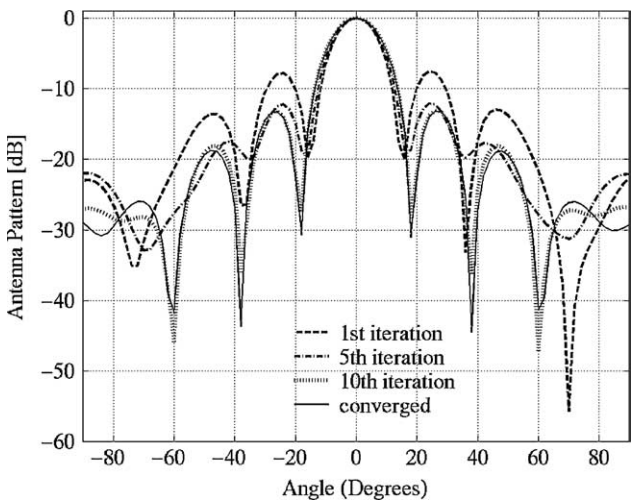

Fig. 11. E-plane antenna patterns of 7×7 Vivaldi antenna array at various DDM iterations–Jacobi iteration.

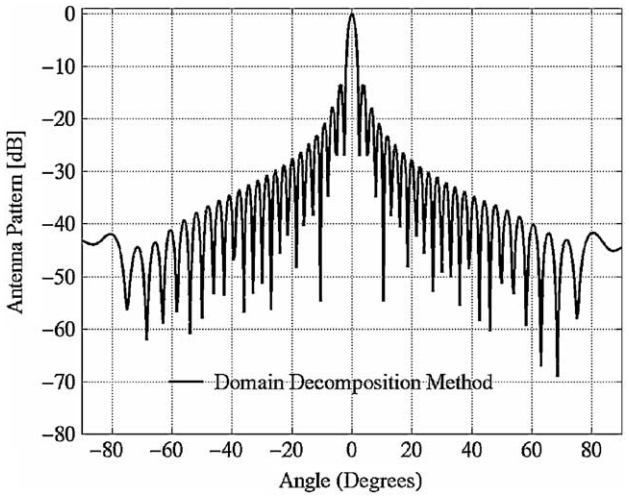

Fig. 12. E-plane antenna pattern of a 50×50 Vivaldi antenna array.

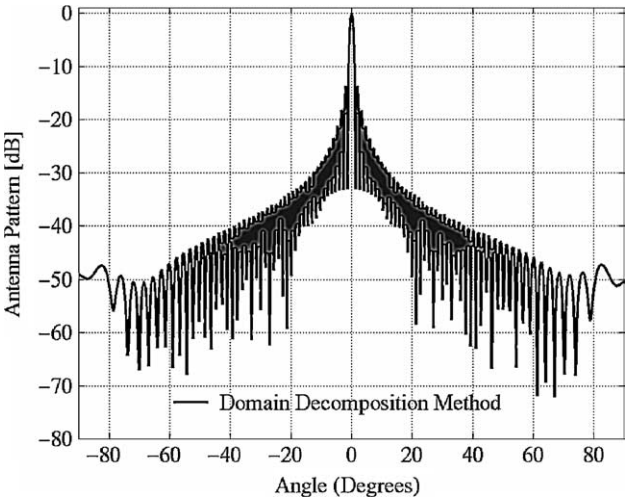

Fig. 13. E-plane antenna pattern of a 100×100 Vivaldi antenna array.

ments Vivaldi arrays were calculated using the DDM and the results are presented in Figs. 12 and 13. In Table 3, some of the statistics for each simulation are tabulated. In the last column, the number of iteration for the Gauss–Seidel is reported for 10^{-1} residual tolerance. For all computations in Table 3, a 2.4 GHz CPU and 2 GByte RAM LINUX PC was used. As summarized in Table 3, 50×50 and 100×100 element Vivaldi arrays required approximately 27 and 108 million unknowns, and 0.47 and 1.65 GB memory, respectively. The computation time was linearly increased as the number of unknowns was increased. Note that for large sized arrays, the memory consumption is dominated only by the storage of the unknown vector. Therefore, the use of the DDM easily solves array problems upward of 100 million unknowns on a common PC with 2 GByte RAM.

Table 3
Computational statistics of DDM and FEBI for various Vivaldi antenna array simulations

Size of array	FEBI		DDM			
	Unknowns	Memory (MB)	Unknowns	Memory (MB)	Time/iteration (h:min:s)	Number of iteration
3×3	80,718	190	98,010	11	00:00:14	17
7×7	528,420	585	533,610	17	00:01:19	19
10×10	1,327,790	1452	1,089,000	26	00:02:25	19
50×50	–	–	27,225,000	471	01:18:47	23
100×100	–	–	108,900,000	1650	04:53:54	23

4. Conclusions

A non-overlapping DDM was successfully formulated and applied to analyze large finite antenna arrays. Robin type TCs were used to speed up the convergence of DDM. The convergence of non-overlapping DDM was investigated through Fourier analysis. In the analysis, it was shown that a complex Robin constant with a positive imaginary part insures the convergence of the propagating modes. However, the evanescent modes of either TE or TM modes fail to converge depending on the sign of the real part in the Robin constant. Additionally, non-matching grids between neighboring sub-domains could be "glued" together with the proposed method, which could relax the restriction on mesh generation process. Using DDM, the geometric repetition was easily utilized, which resulted in a dramatic reduction of computational resources. We first validated the proposed method through small Vivaldi arrays, by comparing the computed antenna patterns with those of the FEBI method. The method was further applied to large sized arrays such as 100×100 elements array in a single PC. It was shown that DDM could be especially efficient for large finite arrays, which have repeating geometric structures.

Acknowledgements

The authors would like to thank Ansoft Corporation in Pittsburgh and Temasek Laboratory, National University of Singapore in Singapore for supporting this work. They extend their thank to an anonymous reviewer for suggesting the link to [36].

References

[1] J. Jin, The Finite Element Method in Electromagnetics, X, second ed., IEEE Press, New York, 2002.
[2] D. Colton, R. Kress, Integral Equation Methods in Scattering Theory, Wiley, New York, 1983.
[3] A. Taflove, Computational Electrodynamics: The Finite-Difference Time-Domain MethoArtech House, Artech House, Boston, 1995.
[4] B. Smith, P. Bjørstad, W. Gropp, Domain Decomposition Parallel Multilevel Methods for Elliptic Partial Cambridge University Press, Cambridge University Press, New York, 1996.
[5] M. Gander, L. Halpern, F. Nataf, Optimized Schwarz methods, in: Proceedings of the 12th International Conference on Domain Decomposition Methods, Chiba, Japan, 2001, pp. 15–26.
[6] M. Gander, F. Magoulès, F. Nataf, Optimized Schwarz methods without overlap for the Helmholtz equation, SIAM J. Sci. Comput. 24 (1) (2002) 38–60.
[7] J.-D. Benamou, B. Després, A domain decomposition method for the Helmholtz equation and related optimal control problems, J. Comput. Phys. 136 (1997) 68–82.
[8] H.A. Schwarz, Uber einige Abbildungsdufgaben, J. Reine Angew. Math. 70 (1869) 105–120.
[9] A. Quarteroni, A. Valli, Domain Decomposition Methods for Partial Differential Equations, Oxford University Press, New York, 1999.

[10] Q. Deng, An optimal parallel nonoverlapping domain decomposition iterative procedure, SIAM J. Numer. Anal. 41 (3) (2003) 964–982.
[11] P.-L. Lions, On the Schwarz alternating methods III: A variant for nonoverlapping subdomains, in: T.F. Chan, R. Glowinski, J. Periaux, O.B. Wildlund (Eds.), Third International Symposium on Domain Decomposition Methods for Partial Differential Equations, SIAM, Philadelphia, 1990, pp. 202–223.
[12] A. Piacentini, N. Rosa, An improved domain decomposition method for the 3D Helmholtz equation, Comput. Methods Appl. Mech. Engrg. 162 (1998) 113–124.
[13] B. Després, Méthodes de décomposition de domaine pour les problémes de propagation d'ondes en régime harmonique, Ph.D dissertation, Paris, 1991.
[14] B. Després, P. Joly, J.E. Roberts, A Domain Decomposition Method for the Harmonic Maxwell Equations in Iterative Methods in Linear Algebra, North-Holland, Amsterdam, 1992, pp. 245–252.
[15] F. Collino, G. Delbue, P. Joly, A. Piacentini, A new interface condition in the non-overlapping domain decomposition method for the Maxwell equations, Comput. Methods Appl. Mech. Engrg. 148 (1997) 195–207.
[16] B. Stupfel, M. Mognot, A domain decomposition method for the vector wave equation, IEEE Trans. Antennas Propagat. 48 (5 (May)) (2000) 653–660.
[17] T. Arbogast, I. Yotov, A non-mortar mixed finite element method for elliptic problems on non-matching multiblock grids, Comput. Methods Appl. Mech. Engrg. 149 (1997) 255–265.
[18] Y. Achdou, C. Japhet, F. Nataf, Y. Maday, A new cement to glue non-conforming grids with Robin interface conditions: the finite volume case, Numer. Math. 92 (2002) 593–620.
[19] A. Alonso-Rodriguez, R. Hiptmair, A. Valli, Hybrid formulations of eddy current problems, Report UTM 663, Universita Degli Studi Di Trento, Trento, Italy, March 2004.
[20] P. Joly, Variational methods for time-dependent wave propagation problems, in: M. Ainsworth, P. Davis, D. Duncan, P. Martin, B. Rynne (Eds.), Topics in Computational Wave Propagation. Direct and inverse Problems, Lecture Notes in Computational Science and Engineering, vol. 31, Springer, Berlin, 2003, pp. 201–264.
[21] C. Wieners, B. Wohlmuth, The coupling of mixed and conforming finite element discretizations, in: J. Mandel, C. Farhat, X. Cai (Eds.), Domain Decomposition Methods, vol. 10, Boulder, 1998, pp. 453–459, August 1997.
[22] C. Bernardi, Y. Maday, A. Patera, A new nonconforming approach to domain decomposition: the mortar element method, in: H. Brezis, J. Lions (Eds.), Nonlinear partial differential equations and their applications, Pitman, 1994, pp. 13–51.
[23] B.I. Wohlmuth, Discretization Methods and Iterative Solvers Based on Domain DecomposiSpringer-Verlag, Springer, Berlin, 2001.
[24] J.-C. Nèdèlec, Mixed finite elements in R3, Numer. Math. 35 (May) (1980) 315–341.
[25] J.F. Lee, D.K. Sun, pMUS (p-type Multiplicative Schwarz) method with vector finite elements for modeling three-dimensional waveguide discontinuities, IEEE Trans. Microwave Theory Tech. 52 (March) (2004) 864–870.
[26] R. Hiptmair, Multigrid method for Maxwell's equations, SIAM J. Numer. Anal. 36 (1998) 204–225.
[27] D.K. Sun, Z.J. Cendes, J.F. Lee, Adaptive mesh refinement, h-version, for solving multiport microwave devices in three dimensions, IEEE Trans. Magn. 36 (4 (July)) (2000) 1596–1599.
[28] A.F. Peterson, Absorbing boundary conditions for the vector wave equation, Microwave Opt. Tech. Lett. 1 (April) (1998) 62–64.
[29] P.A. Raviart, J.M. Thomas, A mixed finite element method for second order elliptic problems, in: I. Galligani, E. Magenes (Eds.), Mathematical Aspect of the Finite Element Method, Lecture Notes in Mathematics, vol. 606, Springer, New York, 1977.
[30] J.D. Jackson, Classical Electrodynamics, third ed., Wiley, New York, 1999.
[31] R.E. Collin, Field Theory of Guided Waves, second ed., IEEE Press/Oxford University Press, Piscataway, 1991.
[32] T. Uwano, T. Itoh, Spectral Domain Approach, in: T. Itoh (Ed.), Numerical Techniques for Microwave and Millimeter-Wave Passive Structures, Wiley, New York, 1989.
[33] A. Sommerfeld, Partial Differential Equations in Physics, Academic Press, New York, 1949.
[34] M.N. Vouvakis, S.-C. Lee, J.-F. Lee, A symmetric FEM-IE formulation with a single-level IE-QR algorithm for solving electromagnetic radiation and scattering problems, IEEE Trans. Antennas Propagat., in press.
[35] H. Holter, H. Steyskal, Some experiences from FDTD analysis of infinite and finite multi-octave phased arrays, IEEE Trans. Antennas Propagat. 50 (12 (December)) (2002) 1725–1731.
[36] Ana Alonso-Rodriguez, Luca Gerardo-Giorda, New non-overlapping domain decomposition methods for the harmonic Maxwell system, Report R.I. N^0 529, Ecole Polytechnique, April 2004.